Geophys. J. Int. (2010) **183,** 407–420 doi: 10.1111/j.1365-246X.2010.04743.x

Automatic computation of moment magnitudes for small earthquakes and the scaling of local to moment magnitude

Benjamin Edwards, Bettina Allmann, Donat Fäh and John Clinton

Schweiz. Erdbebendienst, Sonneggstrasse 5, 8092 *Zürich, Switzerland. E-mail: edwards@sed.ethz.ch*

Accepted 2010 July 16. Received 2010 July 15; in original form 2009 July 16

SUMMARY

Moment magnitudes (M_W) are computed for small and moderate earthquakes using a spectral fitting method. 40 of the resulting values are compared with those from broadband moment tensor solutions and found to match with negligible offset and scatter for available M_W values of between 2.8 and 5.0. Using the presented method, M_W are computed for 679 earthquakes in Switzerland with a minimum $M_L = 1.3$. A combined bootstrap and orthogonal L1 minimization is then used to produce a scaling relation between M_L and M_W. The scaling relation has a polynomial form and is shown to reduce the dependence of the predicted M_W residual on magnitude relative to an existing linear scaling relation. The computation of M_W using the presented spectral technique is fully automated at the Swiss Seismological Service, providing real-time solutions within 10 minutes of an event through a web-based XML database. The scaling between M_L and M_W is explored using synthetic data computed with a stochastic simulation method. It is shown that the scaling relation can be explained by the interaction of attenuation, the stress-drop and the Wood–Anderson filter. For instance, it is shown that the stress-drop controls the saturation of the M_L scale, with low-stress drops (e.g. 0.1–1.0 MPa) leading to saturation at magnitudes as low as $M_L = 4$.

Key words: Fourier analysis; Inverse theory; Earthquake ground motions; Earthquake source observations; Seismic attenuation.

1 INTRODUCTION AND BACKGROUND

The computation of moment magnitudes (M_W) of small earthquakes ($M_W < 3.5$) is not a routine procedure at observatories such as the Swiss Seismological Service (SED). Classical determination of M_W using moment tensor solutions (e.g. Bernardi *et al*. 2004; Clinton *et al*. 2006), hereinafter referred to as M_W(MT), relies upon the availability of long period data (e.g. greater than 5 s). As such it is limited by a minimum magnitude threshold, above which the recorded ground motions at these long periods are routinely stronger than the background noise. This minimum magnitude is typically in the range of M_W 3.5–4 for local events, but depends on the density of stations and the event location.

For regions of low-to-moderate seismicity, the determination of M_W for small events is desirable to obtain robust *a* and *b* values in a recurrence relationship and the magnitude of completeness of the earthquake catalogue (Woessner & Wiemer 2005). Typically, M_L is converted to M_W using a simple scaling relation derived from the larger events (where both magnitudes can be independently determined). In addition, although the use of small earthquakes in deriving empirical ground–motion relationships is strongly debated, their use may lead to more realistic predictive equations that capture features that scale with magnitude, for instance, the magnitude dependence of geometrical spreading (Cotton *et al*. 2008). The use of poor meta-data, such as M_W inappropriately scaled from M_L, for small-magnitude events introduces a significant uncertainty in the prediction of ground–motion at low magnitudes (e.g. Bommer *et al*. 2007). To extend the available magnitude range for empirical ground–motion relationships, the direct determination (or appropriate conversion) of M_W for small earthquakes is therefore vital. The work detailed in this article forms the basis of the scaling relation used to create a homogenized magnitude scale for the earthquake catalogue of Switzerland 2009 (ECOS09), which is an update of the previous catalogue, ECOS02 (Fäh *et al*. 2003a). Extensions of the scaling relation to lower and higher magnitudes than those covered in the scope of this paper will be published elsewhere.

The Swiss Seismological Service (SED) is responsible for the operation and maintenance of a large digital broadband seismic network in Switzerland (SDSNet) in addition to a large strong-motion network (SSMNet). Collectively, these two networks are referred to as CHNet. By the end of 2006, CHNet included 52 sites with 64 modern high-quality sensors: 27 three-component Streckeisen STS-2 broadband seismometers; eight three-component Lennartz 5-s LE-3D/5s sensors; one three-component Lennartz 1-s LE-3-D/1s sensor; and 28 three-component Kinemetrics Episensor strong-motion sensors (Baer *et al*. 2007). The network is however, rapidly expanding. In addition to CHNet, several digital broadband instruments of foreign networks operating near the Swiss border region are available for use in real-time. These include instruments of the Italian National Seismic Network, the German Regional Seismic

Network, the Landes Erdbebendienst Baden-Württemberg and the Austrian Broadband Seismic Network. In total, around 80 sites with broadband digital recording instruments are routinely available in Switzerland and its border regions.

Data from the stations of the CHNet and selected stations of the bordering networks are digitally transmitted to a central processing server in real time. Automatic phase picking and hypocentre location is performed as soon as an earthquake is detected. Estimated location, M_L, and pick times are then available within minutes of an earthquake. M_L is calculated following a modification of the original formulation of Gutenburg & Richter's (1954) local magnitude scale:

$$M_L(\mathrm{SED}) = \log A_0 + C_d + C_e, \quad (1)$$

where A_0 is the maximum mean-to-peak horizontal amplitude in millimetres on a synthesized 2800× Wood–Anderson torsion seismometer and C_d is a distance correction, given by

$$C_d = 0.0180\ R + 1.77 \quad \text{for } R = 60 \text{ km}$$
$$C_d = 0.0038\ R + 2.62 \quad \text{for } R > 60 \text{ km} \quad (2)$$

and where R is the epicentral distance in kilometres (Kradolfer 1984). This scaling relation was derived using vertical recordings on short-period instrumentation with analogue telemetry. $C_e = 0.1$ is an empirically derived correction to the scaling relation that was implemented to maintain consistency in the M_L(SED) scale after:

(a) the update of the Swiss seismic network from the original analogue short-period to a broadband digital system. Contribution to C_e is 0.4;

(b) a change to the use of the horizontal component of motion rather than vertical. Contribution to C_e is −0.3.

It is well known that many agencies report different systematic trends in the relation of M_L to M_W. One disadvantage of the M_L scale is that the effects of frequency-dependent attenuation (e.g. due to scattering and intrinsic Q) are only loosely considered by the distance correction. In addition, the distance term is often calibrated to southern California (although not in the case of Switzerland) and does not consider effects that could be regionally variable, such as Q or stress-drop (Deichmann 2006).

M_W is defined to be proportional to the seismic moment (M_0) measured in Nm. This is itself related to the fault area, A, the average slip across the fault, d, and the shear strength of the rock, μ, by

$$M_W = 2/3 \log(M_0) - 6.03 = 2/3 \log(\mu A d) - 6.03. \quad (3)$$

This measure of magnitude is independent of the attenuation effects previously described (Hanks & Kanamori 1979). It is therefore useful to provide this measure of magnitude alongside the traditional M_L. Currently, the SED operates an automatic real-time moment tensor inversion for local earthquakes (Clinton *et al*. 2006), which is based on the method of Dreger (2003). The automatic M_W(MT) solution is typically available within 15 minutes of the event. However, they are only available for larger earthquakes (i.e. greater than M_L 3.5–4) due to the presence of noise at low frequencies for smaller events.

It has long been known that the seismic moment, M_0, of an earthquake can be related to the long-period spectral plateau of earthquake spectra (e.g. Brune 1970; 1971; Eshelby 1957; Madagaria 1976). Although the seismic moment is related to the long-period spectral level, for small earthquakes (i.e. $M_W < 3$) the 'long-period' plateau is actually present at fairly high frequencies: for an earthquake with $M_W = 3$ and stress-drop of 10 MPa the theoretical corner-frequency is around 10 Hz. Furthermore, the corner-frequency increases inversely proportional to the cube of the seismic moment for a constant stress-drop, such that even though smaller events suffer more due to low-frequency noise, the plateau is present at higher and higher frequencies. As a result, the robustness of the determination of the long-period spectral level is good even for small earthquakes where the background noise dominates the recording at low frequencies. Following previous work of Ottemöller & Havskov (2003), Edwards *et al*. (2008), Edwards (2008) and Edwards & Rietbrock (2009) it is shown that a robust determination of M_W is possible using spectral fitting methods and the instantaneous slip model of Brune (1970, 1971). The method has been improved and targeted specifically at computation of M_W, hereinafter referred to as M_W(SP), at the SED. In addition, the process is fully automated by checking for new earthquake data (automatic pick and location) and updating an XML database with any solutions within five minutes.

This paper is presented in three main parts. The first section describes the derivation of M_W for small and moderate earthquakes in Switzerland using a spectral fitting method, including a comparison with existing M_W(MT) values computed using a moment tensor inversions. In the second section, we use the new M_W(SP) to define a M_L to M_W scaling relation over the range of M_L values from 1.3 to 5.4. In the final section, we try to understand the observed scaling relation in terms of source and path effects using synthetic data.

2 COMPUTATION OF M_W FROM EARTHQUAKE SPECTRA

2.1 Data processing

Data processing and quality control play a crucial role in the determination of M_w using spectral fitting techniques. It is particularly important for small earthquakes, where the background seismic noise, rather than the earthquake, dominates the low-frequency spectral amplitudes. The data collection and processing approach used in this study is as follows: the waveforms are first windowed to provide data that are categorized as signal and noise: one of each being necessary for each record. As *S*-wave arrivals are not automatically picked, a *P*:*S* ratio of 1.73 is used to estimate the arrival time from the automatic *P*-wave picks. The signal window initially starts 5 s before the *S*-pick and is composed of unclipped data of at least 10 s, and at most 50 s in duration, depending on the availability of data. This initial window is then refined, following the method proposed by Raoof *et al*. (1999) to encapsulate 5–75 per cent of the cumulative squared velocity of the record. After this procedure, the signal windows usually start at the *S*-wave arrival with lengths that are significantly shorter than the original maximum of 50 s, dependent on the source–station distance. This approach also means that the results are relatively insensitive to the pick-times of the *P* and *S* waves, and in addition, provides a quantitative measure of shaking duration based on the cumulative squared velocity for potential further analysis. An example of data from one of the stations used in this paper is shown in Fig. 1.

Following the selection of the signal window, a pre-*P*-wave noise window is selected. Its duration is chosen to be as long as possible to enable the correct recovery of any long-period noise. Specifically, the noise window starts at the beginning of the trace, and continues over a duration equal to 75 per cent of the time until the *P*-wave arrival. This ensures that potentially inaccurate *P*-wave arrival time picks (or estimates) do not lead to the noise window being contaminated by the *P*-arrival. It should be noted that for events recorded

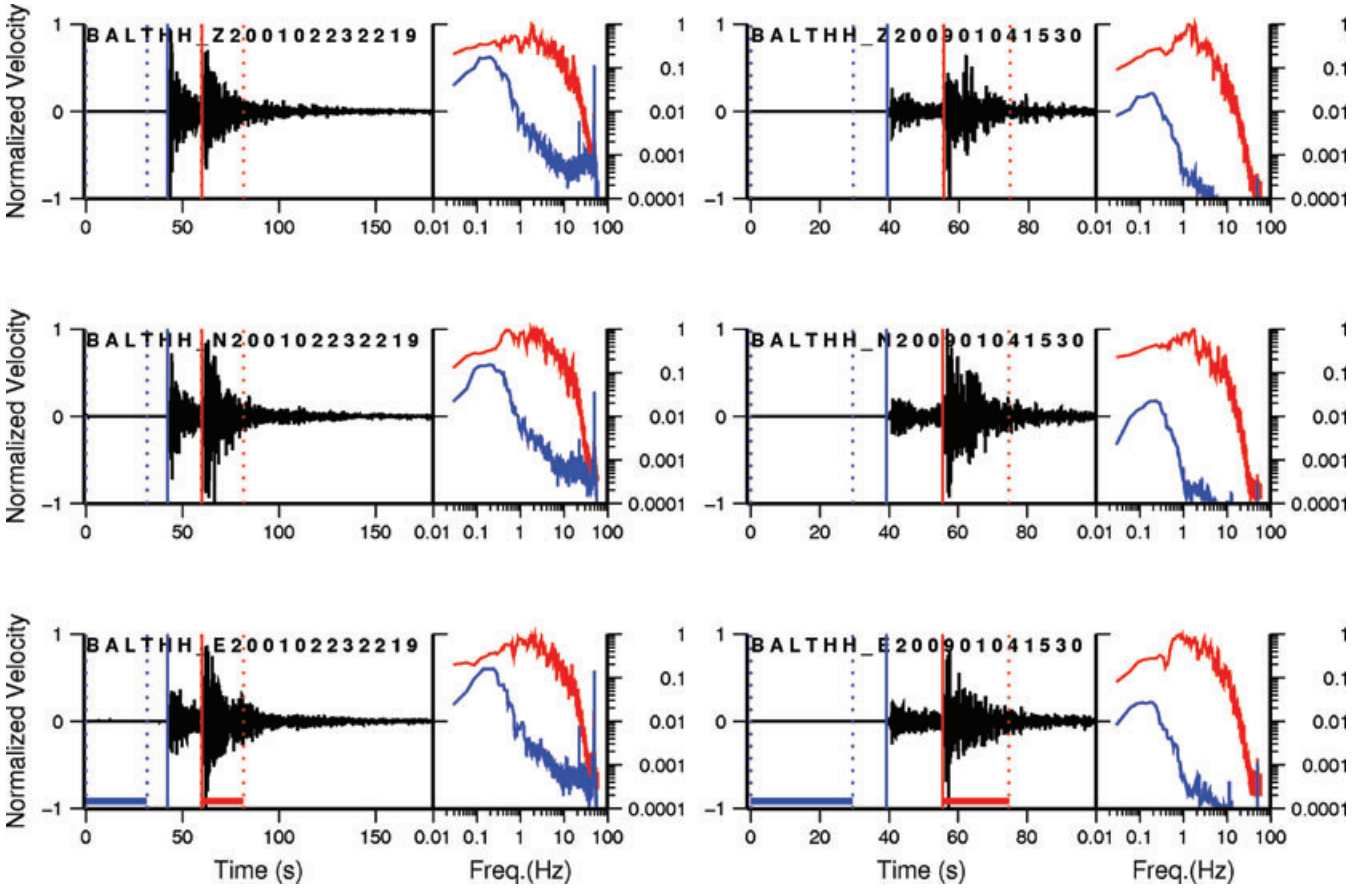

Figure 1. Three-component velocity data from station BALST for two events. Left panel: 2001 February 23, $M_L = 3.6$ event. Right panel: 2009 January 4, $M_L = 4.1$ event. For each event, the normalized three-component velocity time-series showing *P* and *S* arrival times (solid vertical lines) and the extent of the signal and noise windows (horizontal lines and dotted vertical lines) are plotted. In this case it is shown that the signal window starts at the *S*-wave arrival time rather than 5 s before due to the removal of the first 5 per cent of cumulative squared velocity. In addition, the corresponding Fourier velocity spectra (normalized to a peak spectral velocity of unity) for the signal and noise are plotted for each channel.

near to the source, the *P*-coda may contaminate the signal window. As we estimate the noise level using data prior to the event, this may lead to an underestimation of the noise level. However, as described later in the paper, we conservatively increase the estimated noise level to account for any underestimation. Zero padding is then used to create equal length windows (signal and noise), and provide the 2^n samples required for the Fast Fourier Transform (FFT). Both signal and noise windows (excluding the zero padding) are then demeaned and tapered using multitaper algorithms (Park *et al*. 1987; Lees & Park 1995) with 5–3π prolate tapers, before applying an FFT and multiplying by the sampling period to obtain the two-sided continuous Fourier velocity spectrum of each record. To account for different window lengths used for the signal and noise spectra and the subsequent zero-padding, the noise spectra are also normalized by $N_{\text{signal}}/N_{\text{noise}}$, where N is the number of points in the time-series (excluding the zero-padding). For accelerometric records, the spectral data are integrated by dividing by iω. All data are then corrected to records of ground–velocity through deconvolution with the complex instrument response function.

To extract only the most reliable data, the noise estimate is automatically increased to insure intersection of the signal and noise at both the lowest and highest frequencies of each spectrum. Although this may reduce the available bandwidth above the signal-to-noise ratio, it prevents unwanted effects from being included in the data. For instance, this includes effects due to the lack of periodicity due to trends in the time-series, the high variance of low-frequency spectral levels for relatively short window lengths, the time-dependence of the noise, or the presence of *P*-coda in the signal window. The useful frequency range is then defined for each recording as where the signal-to-noise ratio is greater than 3 over a continuous bandwidth of at least 1 $\log_{10}$ units of frequency (e.g. 1–10 Hz or 0.5–5 Hz). For inclusion in the spectral inversion, only frequencies up to 30 Hz are considered.

2.2 Inversion model formulation

A simplification of the method detailed in Edwards *et al*. (2008) and Edwards & Rietbrock (2009) is applied to the data in order to robustly determine M_W using the following model of the Fourier velocity spectrum:

$$\Omega_{ij}(f, r) = 2\pi f E_i(f, f_{ci}) B_{ij}(f, t^*_{ij}) S_{ij}(r, r_{0\ldots n-1}, \lambda_{1\ldots n}) \times T_j(f, A_j) I_j(f), \quad (4)$$

where $E_i(f, f_{ci})$ is the (Brune 1970, 1971) source model for event i with a defining corner-frequency f_c, $B_{ij}(f,t^*_{ij})$ is the attenuation along the ray path

$$B_{ij}(f) = \mathrm{e}^{-\pi f t^*_{ij}}, \quad (5)$$

where t^*_{ij} is the frequency independent whole path attenuation operator (both crustal and site attenuation), which is sometimes

separated into a crustal attenuation parameter t^* and site attenuation parameter κ (e.g. Anderson & Hough 1984) and is defined by

$$t^*_{ij} = \frac{t_{ij}}{Q_{ij}}, \tag{6}$$

where t_{ij} is the traveltime and Q_{ij} is the path-dependent dimensionless quality factor (Rietbrock 2001). It should be noted that due to the relatively long window lengths used (encapsulating the duration of significant shaking), the degree of attenuation may vary at different points in the window due to different paths and travel times of the individual phases. In this case, therefore the attenuation parameter, t^*_{ij}, obtained from inversion will describe the average attenuation over all the travel paths (e.g. $Q_{\rm LG}$; Ottemöller 2002). $S_{ij}(r, r_{0,\dots,n-1}, \lambda_{1,\dots,n})$ is the amplitude decay with distance or 'apparent geometrical spreading', given by

$$S_{ij}\,(r, r_{0\dots n-1}, \lambda_{1\dots n}) = \begin{cases} \left(\dfrac{r_0}{r}\right)^{\lambda_1} & r \le r_1, \\ S\,(r_1)\left(\dfrac{r_1}{r}\right)^{\lambda_2} & r_1 \le r \le r_2, \\ \vdots & \vdots \\ S\,(r_n)\left(\dfrac{r_n}{r}\right)^{\lambda_n} & r \ge r_n, \end{cases} \tag{7}$$

where r is the hypocentral distance, $r_{n>0}$ are distances at which the rate of decay changes from the λ_n to the λ_{n+1} decay value, and r_0 is the rupture radius, which can be normalized to $r_0 = 1$ km without affecting $M_{\rm W}$(SP) as long as $r_0 = 1$ km is maintained in eq. (13). $T_j(f, A_j)$ is the site transfer function (including the generic 'rock-amplification' due to increasing velocity with depth (e.g. Boore & Joyner 1997) at the recording station which is given by

$$T_j(f,\ A_j) = A_j a_j(f), \tag{8}$$

where A_j is the average site amplification and $a_j(f)$ the normalized frequency-dependent site amplification, relative to a reference site (that may not necessarily be known). Finally, $I_j(f)$ is the instrument response function which is set to $I_j(f) = 1$ as the response of the instrument is removed from the data prior to the inversion.

In this paper, we refer to the signal moment, which is the far-field long period spectral amplitude, or the frequency-independent parameters in eq. (4). It is defined as

$$\hat{\Omega}_{ij} = \Psi_i A_j S_{ij}(r, r_{0,\dots,n-1}, \lambda_{1,\dots,n}), \tag{9}$$

where $S_{ij}(r, r_{0,\dots,n-1}, \lambda_{1,\dots,n})$ is given by eq. (7), A_j is the site amplification parameter independent of frequency, and Ψ_i is the effective long period plateau value at the source location.

2.2.1 Inversion procedure

The inversion approach is summarized as follows. First, an initial inversion of the spectra is performed for three defining parameters—the source corner-frequency (f_c) of the Brune (1970) far-field source spectrum, the signal moment (the frequency-independent far-field amplitude) and path-dependent Q_{ij}. The inversion routine implements a combined grid-search for f_{ci} and Powell's minimization for $t_{ij}{}^*$ and the signal moment (Press *et al*. 1997). The grid search of f_{ci} is performed at 10 per cent intervals, starting at the equivalent f_c value for a 0.001 MPa approximate stress-drop and increasing to at the equivalent f_c for a 100 MPa approximate stress-drop, such that the nth grid-search value of f_c is given by

$$f_{c,n} = 1.1^n\left(0.4906\ \beta\left(\Delta\sigma_{\rm min}/10^{(1.5{\rm ML}+9.1)}\right)^{1/3}\right) \ \text{for } n = 1, 2, 3, \dots \tag{10}$$

while

$$f_{c,n} < \left(0.4906\ \beta\ \left(\Delta\sigma_{\rm max}/10^{(1.5\ {\rm ML}+9.1)}\right)^{1/3}\right) \tag{11}$$

with $\Delta\sigma_{\rm min} = 0.001$ MPa, $\Delta\sigma_{\rm max} = 100$ MPa and $\beta = 3500$ ms^{-1}. Note that an assumption of $M_{\rm L} \approx M_{\rm W}$ is made in eqs (10) and (11) to approximate the starting point of the grid search over f_c (as the $M_{\rm W}$ value is as yet unknown). Note, however, that the wide search range ($0.001 \le \Delta\sigma < 100$ MPa) prevents any bias in results. Each earthquake is assumed to have a common corner-frequency across all recordings. This may not be necessarily the case due to directivity and radiation effects, but it actually provides a stable average consistent with the Brune (1970, 1971) instantaneous slip model. In fact, Mayeda & Walter (1996) found that in the case of shear-wave coda, scattering in the Earth's crust averages out such azimuthal variations. The use of long windows is therefore advantageous in reducing the influence of directivity effects in addition to increasing the reliability of long-period spectral estimation. For the choice of the minimization function, it was found in Edwards *et al*. (2008) and Edwards & Rietbrock (2009) that the log-space least squares fit significantly reduces the covariance between t^*_{ij}, f_{ci} (the source corner-frequency), and the signal moment.

In Edwards *et al*. (2008) and Edwards & Rietbrock (2009), we proceeded to tomographically reconstruct the Q structure using the obtained path-dependent t^*_{ij} values (which represent path-dependent Q_0) to stabilize the inversion and obtain robust determinations of the source corner-frequency and stress-drop. However, it is shown in this study that the initial signal moments (allowing for path variable attenuation and therefore without the need for *a priori* knowledge of attenuation) can be used to successfully compute $M_{\rm W}$ from even small earthquakes without significant trade-off or bias. The decision to allow the attenuation to vary for each path also prevents any bias associated with assuming a constant Q_0 from influencing the $M_{\rm W}$ value. This bias was tested for the 2009 January 4 $M_{\rm L} = 4.1$ event (Table 1) using fixed $Q_0 = 325$, 650 and 1300. This led to a $\Delta M_{\rm W}$ of -0.07 (for $Q_0 = 325$) and $+0.09$ (for $Q_0 = 1300$) from a reference $M_{\rm W}$ computed with $Q_0 = 650$. However, it should be noted that several authors have previously demonstrated that due to the lack of *a priori* knowledge of the attenuation, and the strong trade-off of this with the source corner-frequency (or stress-drop), values of t^*_{ij} and f_{ci} obtained with this unconstrained inversion can be unreliable (e.g. Abercrombie & Leary 1993; Abercrombie 1997; Bay *et al*. 2003; Sonley & Abercrombie 2006; Allmann & Shearer 2007; Edwards *et al*. 2008). In this paper, we focus specifically on the determination of the low-frequency spectral level, used to define $M_{\rm W}$, which was shown to be relatively insensitive to the parameter trade-off using the $M_{\rm L} = 4.1$ event. Nevertheless, to fully assess its effect, the uncertainty of all the parameters is taken into account. We compute parameter uncertainty following the method of Viegas *et al*. (2010): from the grid-search around f_{ci} we find those values that are within 5 per cent of the minimum misfit. The corresponding range of signal moment and t^*_{ij} values are then obtained. The uncertainty in the individual signal moment values are then propagated through the inversion procedure, leading to an error estimate on $M_{\rm W}$ which takes into account the uncertainty in the spectral deconvolution.

A principal difference in the spectral fitting in this study relative to Edwards & Rietbrock (2009) is the application of a weighting parameter to the data, equal to $1/f$. This gives preference to fitting the long-period spectral amplitudes, similar in effect to a log-space resampling in frequency (e.g. Ide *et al*. 2003). The misfit function for a particular spectrum (assuming equal variance in the spectral

Table 1. Events with quality 'A' moment tensor solutions M_W(MT) (Clinton *et al*. 2006), and corresponding M_W(SP) computed in this study.

Year	Month	Day	Time	Lat (°)	Lon (°)	Depth (km)	M_W(SP)	$\pm\sigma$	M_W(MT)	M_L
1999	09	13	2327	45.47	5.49	10	3.31	0.094	3.2	3.6
1999	12	29	2042	46.55	10.30	11	4.93	0.240	4.9	5.1
2000	04	06	1740	46.53	10.36	15	4.13	0.062	4.0	4.3
2000	06	03	1514	47.21	10.10	2	3.62	0.075	3.6	3.9
2000	06	16	1157	45.95	10.82	10	3.51	0.070	3.5	3.9
2000	08	19	0837	46.03	6.68	5	3.39	0.083	3.4	3.4
2001	02	23	2219	46.14	7.03	6	3.51	0.064	3.4	3.6
2001	02	25	0122	46.13	7.03	7	3.19	0.050	3.2	3.1
2001	03	17	0029	46.92	9.01	3	3.50	0.055	3.4	3.8
2001	04	06	0222	45.92	9.28	22	3.54	0.062	3.3	3.3
2001	05	30	2243	45.83	6.53	10	2.89	0.064	3.0	3.1
2001	07	17	1506	46.67	11.09	10	4.71	0.081	4.7	5.0
2001	07	18	2247	44.40	8.72	10	4.07	0.084	4.2	4.2
2001	10	30	1730	47.26	10.17	10	3.10	0.067	3.2	3.1
2003	03	22	1336	48.29	8.98	9	3.99	0.048	3.9	4.4
2003	04	11	0926	44.86	8.92	10	4.57	0.051	4.9	5.0
2003	05	06	2159	46.90	8.91	3	3.67	0.044	3.6	4.0
2003	05	25	2303	45.16	6.49	10	3.44	0.066	3.6	3.5
2003	07	18	1101	46.72	9.84	7	3.52	0.049	3.5	3.9
2003	08	01	0320	46.73	9.84	7	3.70	0.045	3.7	3.9
2003	08	12	0038	46.72	9.83	6	2.84	0.056	2.8	2.9
2003	08	22	0921	46.31	7.33	4	3.70	0.043	3.6	4.0
2004	02	18	1431	46.61	6.99	9	3.18	0.041	3.2	3.3
2004	06	28	2342	47.53	8.17	20	3.51	0.034	3.4	4.0
2004	11	24	2259	45.56	10.62	10	4.86	0.049	5.0	5.3
2004	12	05	0152	48.08	8.00	10	4.57	0.039	4.5	5.1
2005	04	18	1059	44.75	9.41	10	3.76	0.086	3.8	3.8
2005	04	19	0827	44.90	9.78	10	3.34	0.099	3.6	3.3
2005	09	06	0708	47.30	11.52	1	3.11	0.067	3.1	3.1
2006	07	22	1808	45.55	10.20	5	3.10	0.067	3.1	3.1
2006	10	20	0011	45.72	10.33	2	3.51	0.045	3.5	3.6
2007	03	23	0501	45.69	9.87	10	3.39	0.050	3.3	3.6
2007	05	19	1619	47.17	10.60	2	3.63	0.034	3.6	3.9
2007	08	19	0732	48.34	6.64	10	3.33	0.071	3.2	3.5
2008	01	21	1640	46.76	9.45	7	3.68	0.030	3.7	4.0
2008	02	17	1241	45.91	7.16	8	3.40	0.035	3.4	3.6
2008	04	17	0107	46.65	10.09	5	3.08	0.040	3.1	3.1
2008	07	14	0351	45.65	10.48	2	3.42	0.050	3.5	3.6
2009	01	04	1530	47.18	9.36	4	3.97	0.031	3.7	4.1

values) is given by

$$\varepsilon_{ij} = \sum_{f_{ij,\mathrm{start}}}^{f_{ij,\mathrm{end}}} \frac{\log\left(\Omega_{ij}^{\mathrm{r}}(f,r)\right) - \log\left(\Omega_{ij}^{\mathrm{m}}(f,r)\right)}{f}, \tag{12}$$

where superscripts r and m denote spectral values for the real data and the model (eq. 4), respectively. $f_{ij,\mathrm{start}}$ and $f_{ij,\mathrm{end}}$ are the minimum and maximum frequencies that define the selected bandwidth for a particular spectrum, respectively. A Powell's minimization (Press *et al*. 1997) is used to solve eq. (12) for each iteration of the grid-search over f_c. The inverted signal moments that correspond to the f_c value leading to the minimum sum of residual misfits, ε_{ij}, over all stations, j, of an event, i, are then extracted.

Having successfully extracted the signal moment (the far-field, long-period spectral displacement amplitude), we can proceed with the deconvolution to find the long-period plateau value at the source by accounting for mean site amplifications and the distance decay function (eq. 9). This is solved using a linear L2 SVD decomposition in the log-space. For fast computation of individual M_W in real-time (i.e. with only the recordings of one event available), the *a priori* knowledge of $S_{ij}(r, r_{0,\ldots,n-1}, \lambda_{1,\ldots,n})$ and A_j must be available. In this case it is assumed that $A_j = 1$ and $S_{ij}(r, r_{0,\ldots,n-1}, \lambda_{1,\ldots,n}) = r^{-1.0}$ for $r < 150$ km and $S_{ij}(r, r_{0,\ldots,n-1}, \lambda_{1,\ldots,n}) = 150^{-1.0}(r/150)^{-0.5}$ for $r \geq 150$ km. The site transfer-term ($T_j(f, A_j)$) was initially taken as that given in Boore & Joyner (1997) for a generic rock-site with $V_{s30} = 620$ ms^{-1}. In addition, a homogeneous half-space model was tested, such that $T_j(f, A_j) = 1$. This resulted in negligible differences in the M_W values (an average of +0.02) compared to those computed when accounting for the generic rock-site site transfer-term of Boore & Joyner (1997). For Switzerland, the average V_{s30} is higher than 620 ms^{-1}, so the true rock amplification lies somewhere in between the Boore & Joyner (1997) generic rock-site and the homogeneous half-space (Poggi *et al.* 2010). We therefore expect the rock amplification effect to be negligible for computing M_W. For simplicity and speed, the half-space model is therefore used. For application in other regions, the average site condition should be assessed and the effect of the site amplification terms considered. However, for NEHRP (BSSC 2003) site classes A and B it is unlikely that any correction is necessary to obtain M_W. For a more physically realistic determination of M_W, for example including the amplification due to Moho reflections, region specific $S_{ij}(r, r_{0,\ldots,n-1}, \lambda_{1,\ldots,n})$ and $T_j(A_j, f)$ can be derived. The reader should refer to Edwards *et al*.

(2008) for a full description of the inversion methodology and the robust determination of these parameters.

It follows that seismic moments can be calculated using the following equation (Brune 1970):

$$M_{0i} = \frac{\Psi_i v^3 \rho r_0 4\pi}{\xi F \Theta_{\lambda\Phi}}, \tag{13}$$

where M_{0i} is the seismic moment (in SI units), Ψ_i is the effective long-period plateau displacement at source i (from eq. 9), $\Theta_{\lambda\Phi}$ is the average radiation pattern ($\Theta_{\lambda\Phi} = 0.55$ for S waves; Aki & Richards 1980; Boore & Boatwright 1984), v is the shear wave velocity at the source (it is assumed that $v = 3.5$ km s^{-1}), F is the free surface amplification ($F = 2.0$ for normally incident SH waves and a good approximation for SV) and ρ is the average crustal density ($\rho = 2800$ kg m^{-3}). r_0 is the fault radius, or 1 km, depending on the definition used in eq. (9). ξ is an empirically derived factor to account for the difference in the horizontal and vertical ground–motion amplitudes if using vertical recordings (in this case $\xi = 1$ as we use only horizontal records) (Newmark & Hall 1982). The use of the average radiation effect coefficient, $\Theta_{\lambda\Phi,}$ relies upon a good range of azimuthal coverage when analysing individual phases, at least over one continuous half of the radiation pattern (due to its symmetry). However, the use of multiply scattered waves reduces the effect of the radiation pattern (e.g. Mayeda & Malagnini 2010) such that the azimuthal coverage is less important. The effect of fault orientation was discussed in Boore & Boatwright (1984) where it was shown that for close observations of a vertical strike slip, 30° dip-slip and 45° oblique slip fault the average radiation coefficients for S waves were 0.50, 0.64 and 0.57, respectively. This would lead to ΔM_W of 0.03 for the vertical strike slip event, −0.04 for the dip-slip event and 0.01 for the oblique dip-slip event. A possible extension of the method could be to follow work such as Kisslinger (1980) and Kisslinger *et al*. (1981) to attempt to obtain an estimate of the focal solution for small events and remove the requirement of an average radiation effect, however, it is likely that this would not be compatible with the real-time application presented here.

3 QUALITY EVALUATION OF M_W FROM SPECTRAL FITTING

3.1 Comparison of M_W

To test the M_W computed using the method described in this paper [referred to as M_W(SP)], a comparison is made with M_W values from automatic moment tensor solutions computed at the SED [M_W(MT)] (Bernardi *et al*. 2004; Clinton *et al*. 2006). 40 earthquakes were selected for comparison, all having the highest category 'A' quality for the M_W(MT) (Table 1). The magnitudes range from M_W(MT) = 2.8 to 5.0. When using broadband full-waveform moment tensor methods, the retrieval of M_W(MT) for small events (e.g. $M_W < 3$) is difficult and only possible when there are nearby recordings and a low level of noise. As a result, moment tensor solutions for small events are not abundant despite their frequent occurrence. The earthquakes used in this comparison are shown in Fig. 2 and Table 1.

The distribution of hypocentral distance and depth of sources with respect to M_L is shown in Fig. 3. In addition, the range of

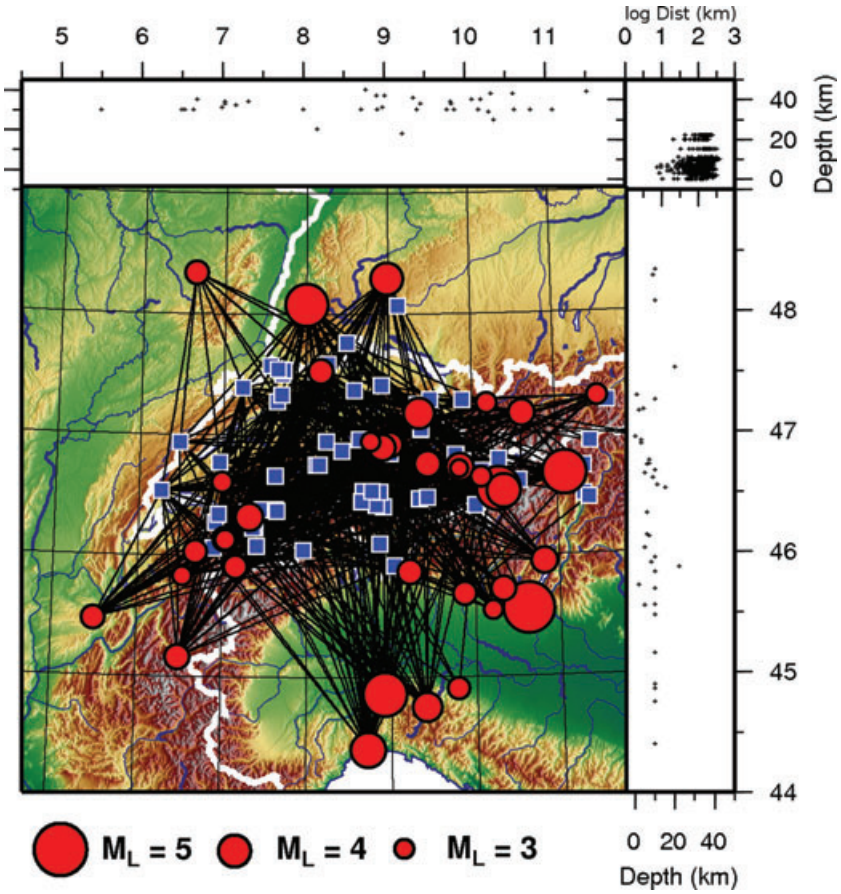

Figure 2. Distribution of earthquakes (circles), instrumentation (squares) and ray-geometry used in the comparison between M_W(SP) and M_W(MT).

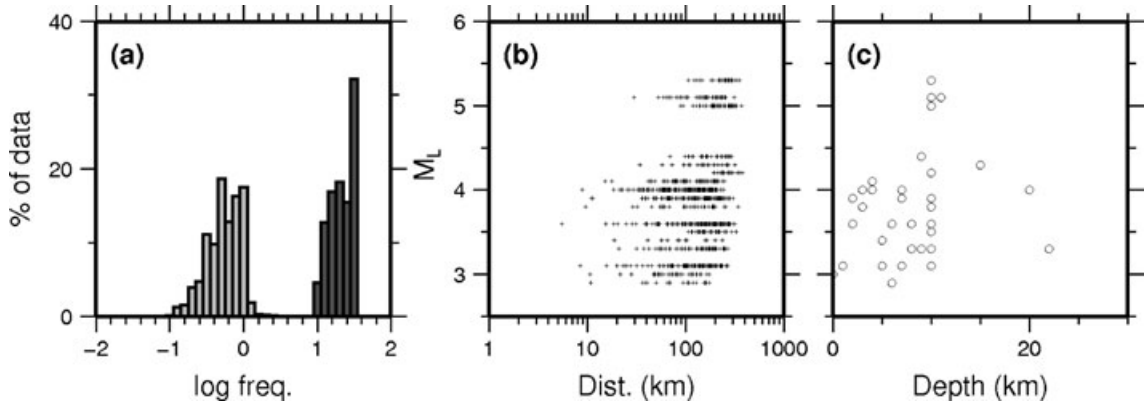

Figure 3. Summary of data used for the comparison of M_W(SP) with M_W(MT): (a) range of minimum (light grey) and maximum (dark grey) frequencies available for the spectral inversion after automatic processing. (b) M_L plotted against the hypocentral distance and (c) M_L plotted against source depth.

minimum and maximum frequencies used in the spectral inversion for M_W(SP) are shown.

The comparison of M_W(MT) with the M_W(SP) derived in this study is shown in Table 1 and Fig. 4. The M_W(SP) were computed using a simple model with $T_j(f, A_j) = 1$ and $S_{ij}(r, r_{0,\ldots,n-1}, \lambda_{1,\ldots,n}) = r^{-1.0}$ for $r < 150$ km and $S_{ij}(r, r_{0,\ldots,n-1}, \lambda_{1,\ldots,n}) = 150^{-1.0}(r/150)^{-0.5}$ for $r \geq 150$ km (i.e. a homogeneous half-space with spherical leading to cylindrical geometrical decay). The error in the M_W(SP) value presented in Table 1 has been propagated through the matrix inversion using the estimates of signal moment variance obtained from the spectral inversion. An example of the spectral fit for the horizontal recordings shown in Fig. 1 is given in Fig. 5. Note that the noise estimate has been increased to intersect the signal at low and high frequencies. This ensures a conservative selection of the useful bandwidth, such that noise does not influence the results. The mean difference between the computed M_W is

$$M_W(\text{SP}) = M_W(\text{MT}) + 0.001 \pm 0.063 \quad (14)$$

as shown in Fig. 4(a). We found that, as most of the large magnitude events occurred at the borders of Switzerland (Fig. 2), a requirement of $\sigma_{azi} > 30$ (the circular standard deviation of source–station azimuths) removes most of the $M_L > 4$ events. Furthermore, the requirement did not lead to any decrease of the misfit between M_W(SP) and M_W(MT).

Following Poggi *et al.* (2010), site transfer functions ($T_j(f, A_j)$) were obtained and removed from the data to check for any improvement in variance or introduction of bias in the M_W(SP) with respect to M_W(MT). In this case however, with generally well recorded events (a minimum of eight stations were available for the smallest events and 29 stations recorded the largest event) the inversion was robust enough that this did not affect the M_W(SP). Where few recordings are available, or for strong systematic site effects (e.g. strong-motion sensors located in a sedimentary basin) the prior-removal of $T_j(f)$ will be necessary for non-biased, robust solutions.

A study of attenuation in Switzerland was performed by Bay *et al*. (2003, 2005) in which they determined $Q_0 = 270f^{0.5}$, and $S_{ij}(r, r_{0,\ldots,n-1,}, \lambda_{1,\ldots,n}) = r^{-1.1}$ for $r < 50$ km; $S_{ij}(r, r_{0,\ldots,n-1,}, \lambda_{1,\ldots,n}) = 50^{-1.1}(r/50)^{-0.6}$ for $50 \leq r < 70$ km; $S_{ij}(r, r_{0,\ldots,n-1,}, \lambda_{1,\ldots,n}) = 50^{-1.1}(70/50)^{-0.6}(r/70)^{0.2}$ for $70 \leq r < 100$ km and $S_{ij}(r, r_{0,\ldots,n-1,}, \lambda_{1,\ldots,n}) = 50^{-1.1}(70/50)^{-0.6}(100/70)^{0.2}(r/100)^{-0.5}$ for $r \geq 100$ km. This attenuation model includes the amplification of ground motion in the range 70—100 km due to S_mS reflections using: $S_{ij}(r, r_{0,\ldots,n-1,}, \lambda_{1,\ldots,n}) = 50^{-1.1}(70/50)^{-0.6}(r/70)^{0.2}$. The model of Bay *et al*. (2003, 2005) was used to compute the same M_W values determined using the simple attenuation model described earlier. However, using the Bay *et al*. (2003, 2005) model, the M_W values are overestimated by an average of 0.1 relative to the M_w(MT) (Fig. 4b). Furthermore, the scatter in the difference between M_W(MT) and M_W(SP) is slightly increased. This could be due to the over-attenuation of low frequencies, or alternatively the incompatibility of the amplitude decay function $S_{ij}(r, r_{0,\ldots,n-1,}, \lambda_{1,\ldots,n})$ with the moment tensor velocity model. To have consistency between the M_W(MT) and M_W(SP) it is therefore better to use the simple model of amplitude decay and to allow attenuation to be path variable. In terms of the individual errors assigned to the M_W values, using the Bay *et al.* (2003, 2005) model significantly reduces these errors. This highlights a problem of using an *a priori* attenuation model, although we reduce the variance of the inverted parameters, we may introduce bias that is difficult to quantify.

4 APPLICATION TO M_L–M_W MAGNITUDE SCALING

4.1 Scaling of M_L–M_W in Switzerland

M_W is the preferred homogeneous measure of magnitude for the Swiss earthquake catalogue (Fäh *et al*. 2003a). Although the method shown here is able to remove the requirement for scaling M_L–M_W for all but the smallest events, it is useful to have scaling relationship for cases where only M_L is available. Previously a simple scaling relation of

$$M_W = M_L(\text{SED}) - 0.2 \quad (15)$$

was used at the SED (Braunmiller *et al*. 2005). This was the result of a regression of 34 events for which both M_W(MT) and M_L(SED) were available. Due to the necessity of having signal above the noise at long periods (e.g. less than 5 s) for computation of broadband M_W(MT), this was limited to the larger events ($M > 3.5$) in the catalogue. This also led to a potential bias in the statistics, as the scaling equation was actually then used outside its valid parameter range: i.e. for $M < 3.5$.

A comparison of M_W and M_L of European earthquakes has been made by of Grünthal *et al*. (2009). They showed that

$$M_W = 0.53 + 0.646\ M_L + 0.0376\ M_L^2. \quad (16)$$

However, this is based on M_L values from a number of catalogues of different seismological agencies, which, as previously mentioned, scale differently. It should, nevertheless represent an average European scaling relation and provide a worthwhile comparison to a unique M_L(SED) to M_W scaling relation.

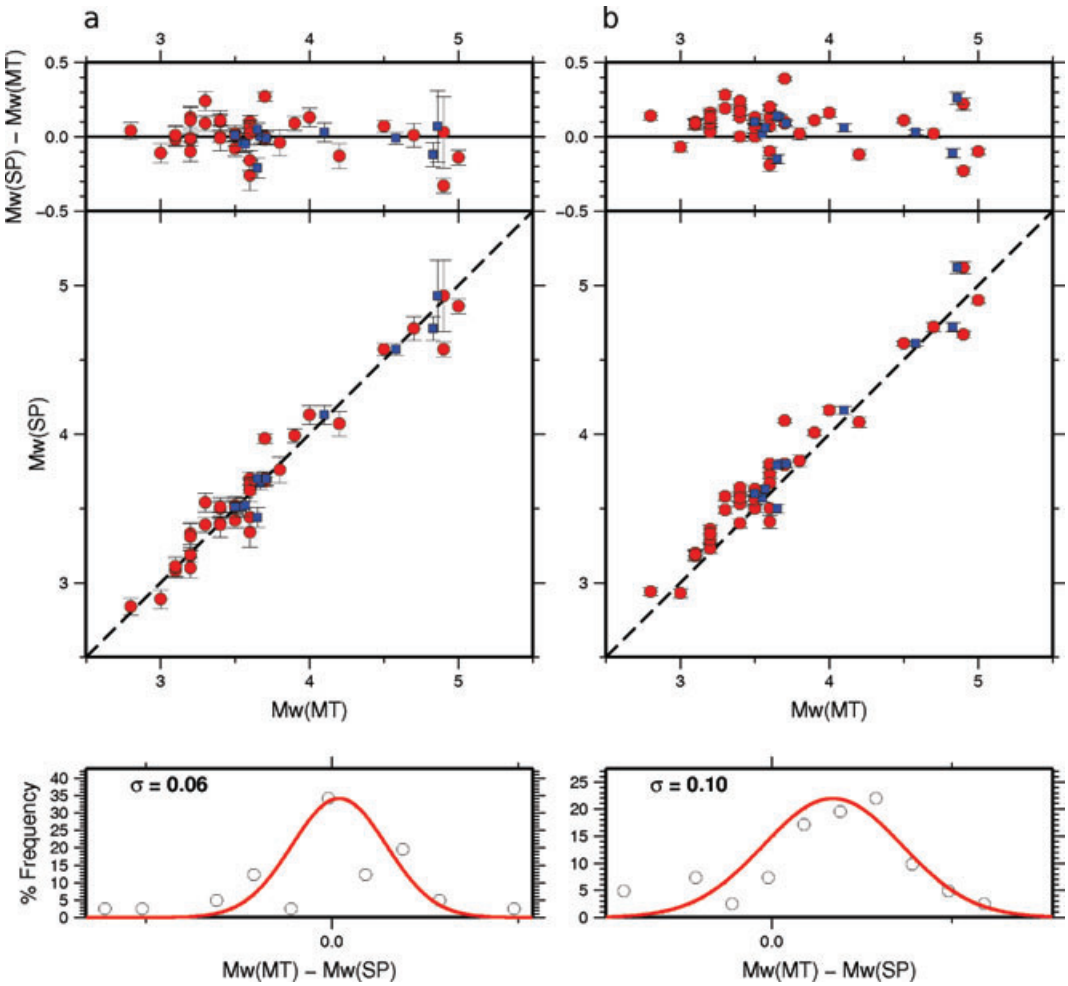

Figure 4. Comparison between the M_W(MT) computed using circles: an automatic moment tensor solution (Clinton *et al*. 2006) and squares: the moment tensor solutions of Bernardi *et al*. (2004) and those computed in this study for (a) path-variable attenuation (b) using the attenuation model of Bay *et al*. (2003, 2005).

The new relation computed in this study is based on M_W(SP) computed using the spectral fitting technique described previously. The quantity of data (679 events) for this regression was substantially larger than the original regression of Braunmiller *et al*. (2005). The minimum magnitude was $M_L = 1.3$. The data were binned into groups of M_L 1–2, 2–3, 3–4 and 4–5.5. A bootstrap technique was used with 1000 subsets comprising of 80 per cent of the full data set, and 20 per cent random repetitions, although enforcing an equal number of data in each M_L bin. This was to evaluate the robustness of the solution and avoid bias due to data selection and magnitude. The regression was an orthogonal L1 solution assuming equal variance in both magnitudes. From the 1000 possible scaling relations given by the bootstrap analysis, a final regression was performed to find the orthogonal L1 solution of the bootstrap possibilities. The new relation is given by

$$M_W = 1.02 + 0.472\ M_L(\mathrm{SED}) + 0.0491\ M_L(\mathrm{SED})^2 \pm 0.15. \quad (17)$$

The range of fits found by the bootstrap approach is shown in Fig. 6. The scaling law of Grünthal *et al*. (2009) (eq. 16) is included for comparison. The scaling relation in this study matches that of Grünthal *et al*. (2009) well for magnitudes greater than $M_L = 3.5$. For lower magnitudes, the scaling relation of this study gives higher M_W for respective M_L values.

It is important to note that the validity of the derived relation does not extend beyond the limits for which data were available: specifically for $M_L > 1.3$ and $M_L < 5.3$ as there is no theoretical basis for a purely quadratic relation between M_L and M_W. This apparent in Fig. 6, where it is shown that the possibilities for the scaling relation grow significantly for $M_L < 1.3$ and $M_L > 5.3$.

4.2 Testing the scaling relation

To test the results of the regression, the M_W(MT) computed by the automatic moment tensor solutions of Clinton *et al*. (2006) are compared with the values predicted by both the old and new scaling relations. These M_W(MT) are completely independent from the M_W(SP) derived for computing the new scaling relation [only M_W(SP) were used] and therefore can provide an unbiased assessment of any residual misfit dependency. The results are shown in Fig. 7. Both the old and new relations tend to underpredict M_W(MT) of events smaller than $M_L = 3.5$–3.75. However, this is due to the fact that, for such earthquakes, it is only possible to obtain high-quality broadband moment tensor solutions for events with particularly high signal-to-noise ratios at nearby recording stations. As a result, M_W values for events with $M_L < 3.75$ tend only to be available for when their M_W is particularly high. Effectively, the

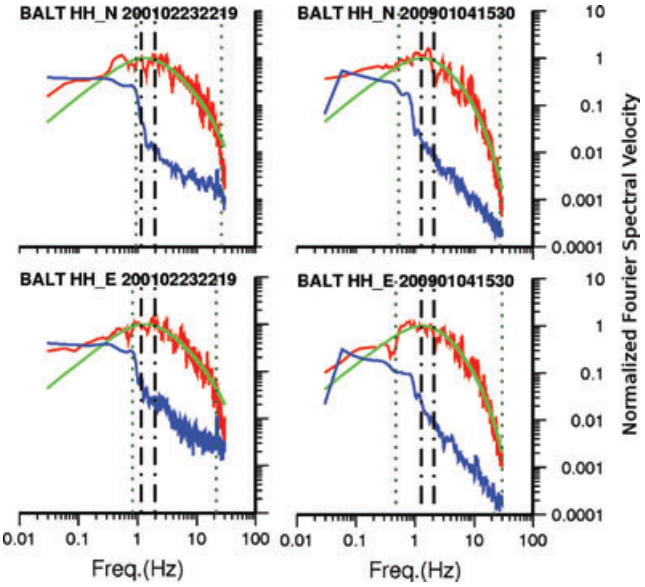

Figure 5. Spectral fit plotted over the normalized input velocity spectra (spectra divided by the peak spectral velocity) for the horizontal components of recording for the events shown in Fig. 1. The top panel shows the north–south and bottom panel the east–west orientations. The adjusted noise estimates are included with the signal data (see text for a description of the noise adjustment). The vertical dotted lines indicate the limits between which the automatic processing selected data for inclusion in the spectral inversion. The vertical dash-dot lines indicate the range of possible f_c based on misfit within 5 per cent of the minimum.

magnitude of statistical completeness for the M_W catalogue of Clinton (personal communication) is around $M_L = 4$ (as a conservative estimate) and statistical interpretation should only be made above this magnitude. For larger earthquakes, there does not seem to be any dependency of the residual misfit on magnitude for either the linear or quadratic relations. Overall there is negligible difference in the M_W residual between the old and new relations for events of $M_L > 3.5$, although the quadratic scaling relation tends to predict higher M_W for $M_L > 4$. The most significant difference between the two scaling relations is at low magnitudes, where it is not possible to independently verify the predictions with M_W(MT).

5 M_L–M_W SCALING SIMULATIONS

In the remaining sections, we attempt to understand the reason for the shape of the observed M_L–M_W scaling relation. Building upon the theoretical framework (e.g. Hanks & Boore 1984; Ben-Zion & Zhu 2002), Deichmann (2006) presented an argument for the scaling of M_L–M_W, where it was shown that, provided the self-similarity of earthquake sources, the scaling of M_L–M_W should be 1:1. The observation that the theoretical 1:1 relationship breaks down in empirical relationships was explored by Hanks & Boore (1984). They postulated that a complex interaction of the Wood–Anderson high-pass filter, the far-field source corner-frequency (of which stress-drop is a proxy; Brune 1970) and the f_{max} (Hanks 1982), requires a polynomial relation to describe the scaling between M_L and M_W. Ben-Zion & Zhu (2002) proposed that an alternative cause of the

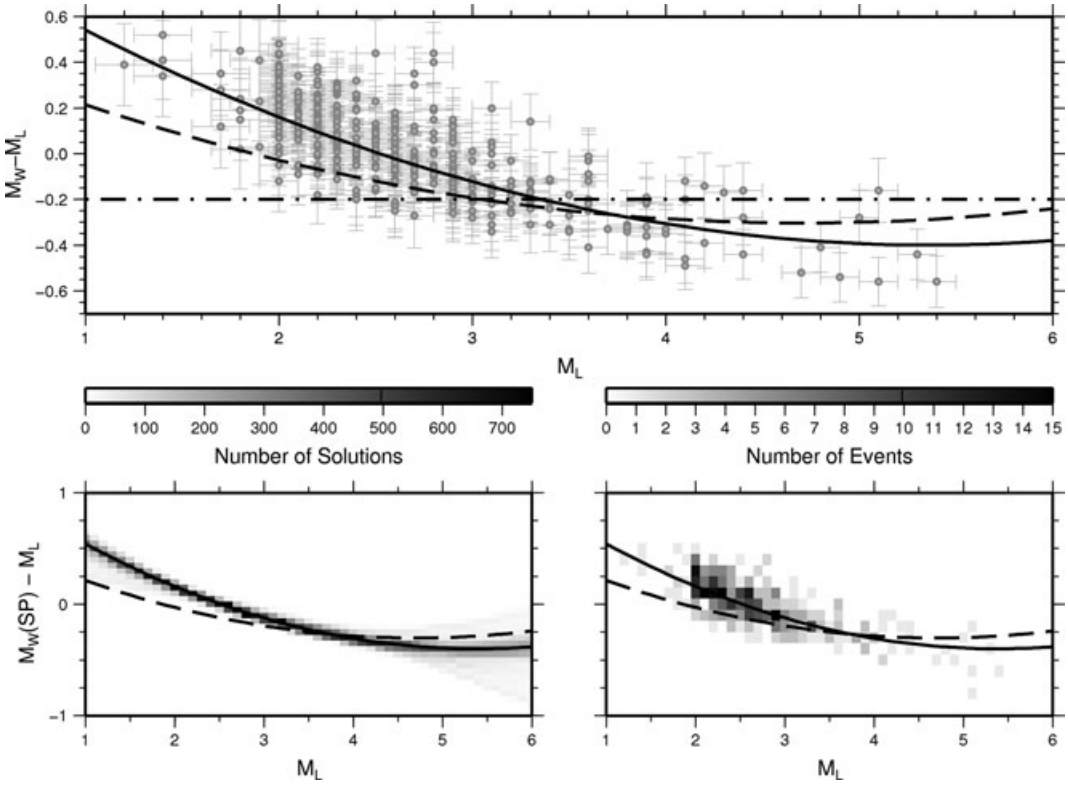

Figure 6. Top panel: plot of all events used to define the scaling relation. The M_L error bars indicate the standard deviation in M_L (σ_{M_L}) as given by the earthquake catalogue of Switzerland (0.15 for $1 \leq M_L < 2$ and 0.1 for $M_L \geq 2$). The M_W–M_L error bars are given by $\sqrt{(\sigma^2_{M_L} + \sigma^2_{M_W})}$. Bottom left: plot of possible polynomial fits found during the bootstrap process to identify the optimal M_L–M_W scaling relationship. Bottom right: density plot of the events used in the bootstrap procedure. The solid lines indicate the best model given by eq. (17), the dash-dot line indicates the old linear scaling relation (eq. 15) while the dashed lines indicate the scaling relation of Grünthal *et al*. (2009).

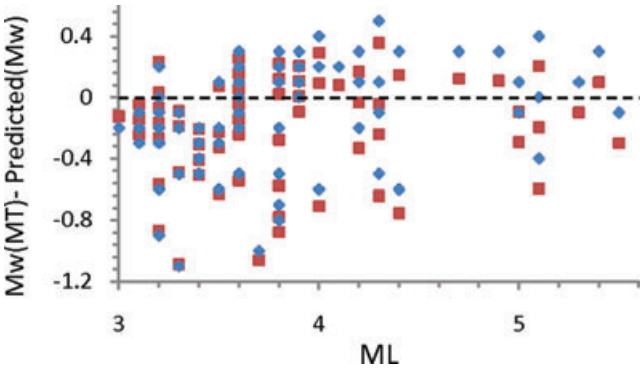

Figure 7. Comparison of M_W (MT) computed by Clinton *et al*. (2006) and those predicted using (squares) the new quadratic and old linear scaling relation (diamonds).

deviation from 1:1 scaling could result from non-self-similarity of earthquake sources. They suggested that a change in the effective stress regime could lead to the observed polynomial scaling between M_L and M_W: for small events the heterogeneity of a tectonic stress-field may lead to slip that does not grow substantially with rupture dimension, whereas for larger events the effect of small scale stress heterogeneities is smoothed out. They suggest that the evolution between the two extremes of small and large events could lead to the observed polynomial form of M_L–M_W scaling (e.g. Miller *et al*. 1999).

To improve our understanding of the influence of attenuation and stress-drop on the scaling of M_L–M_W, scaling relationships were simulated through the generation of stochastic waveforms. Following the method of Boore (2003), accelerograms can be synthesized by convolving the Fourier acceleration spectrum of an earthquake with Gaussian noise shaped with a tapering function. Furthermore, by applying the resulting acceleration time-series to a damped simple harmonic oscillator with properties of the Wood–Anderson Seismometer (damping factor equal to 0.69, natural period of 0.8 s, gain of 2800), the peak Wood–Anderson amplitude can be obtained. Note that to maintain consistency, the properties used to simulate the Wood–Anderson Seismometer response are chosen to match those used for the computation of M_L(SED) rather than the empirically derived response (e.g. Uhrhammer & Collins 1990). The Fourier acceleration spectrum required for the stochastic simulation can be reconstructed using eqs (3), (4) and (13), requiring only the M_W, stress-drop, attenuation, site amplification and duration of shaking, T_d. The source corner-frequency is obtained from the stress-drop using (Boore 2003)

$$f_c = 0.4906\beta \left(\frac{\Delta\sigma}{M_0}\right)^{1/3}, \tag{18}$$

which is based on Brune (1970, 1971) and Eshelby (1957). Attenuation is parameterized in terms of the crustal attenuation, Q, the site attenuation κ (synonymous to the f_{max}; Hanks 1982) and geometrical spreading.

5.1 Bay *et al*. (2003, 2005) attenuation and source scaling model

In a first step, a synthesized M_W versus M_L scaling relation is produced based on the geometrical spreading, Q, stress-drop and κ given by Bay *et al*. (2003). These are $S_{ij}(r,r_{0,\ldots,n-1},\lambda_{1,\ldots,n}) = r^{-1.1}$ for $r < 50$ km; $S_{ij}(r,r_{0,\ldots,n-1},\lambda_{1,\ldots,n}) = 50^{-1.1}(r/50)^{-0.6}$ for $50 \leq r < 70$ km; $S_{ij}(r,r_{0,\ldots,n-1},\lambda_{1,\ldots,n}) = 50^{-1.1}(70/50)^{-0.6}(r/70)^{0.2}$ for $70 \leq r < 100$ km and $S_{ij}(r,r_{0,\ldots,n-1},\lambda_{1,\ldots,n}) = 50^{-1.1}(70/50)^{-0.6}(100/70)^{0.2}(r/100)^{-0.5}$ for $r \geq 100$ km (in the form of eq. 7); constant $\Delta\sigma = 0.5$–1.0 MPa; $Q(f) = 270f^{0.5}$ and $\kappa = 0.015$ s. Site amplification is set to $T(f, A) = 1$ as the model is referenced to an undefined average site condition and the duration of shaking is detailed in Bay *et al*. (2003). M_L values are computed over a range of distances (10, 20, 30, 50, 100 and 200 km) to prevent bias in the computed M_L. The synthesized M_L versus M_W are shown in Fig. 8. It can be seen that M_L synthesized using the model of Bay *et al*. (2003) do not follow the empirical curve. This is consistent with Bay *et al*.'s (2005) findings where it was shown that ground motion tended to be underpredicted using the model with constant stress-drop. In Bay *et al*. (2005), it was proposed that an increasing stress-drop with seismic moment model, such that

$$\Delta\sigma = 0.79 \times 10^{(0.38(MW-4.2))}\ \text{MPa}, \tag{19}$$

along with $\kappa = 0.0125$ s may lead to better estimates of ground–motion at higher magnitudes. Despite the change, the resulting synthesized scaling relation (Fig. 8) still does not adequately match the observed relation. The inadequacy of the Bay *et al*. (2003) and Bay *et al*. (2005) models in synthesizing the observed scaling relation leads us to explore why this is the case. Using a grid-search it was found that the observed scaling relation could be adequately replicated by a synthetic relation (Fig. 8). However, the uncertainty of the model was unacceptably high. In the following section the

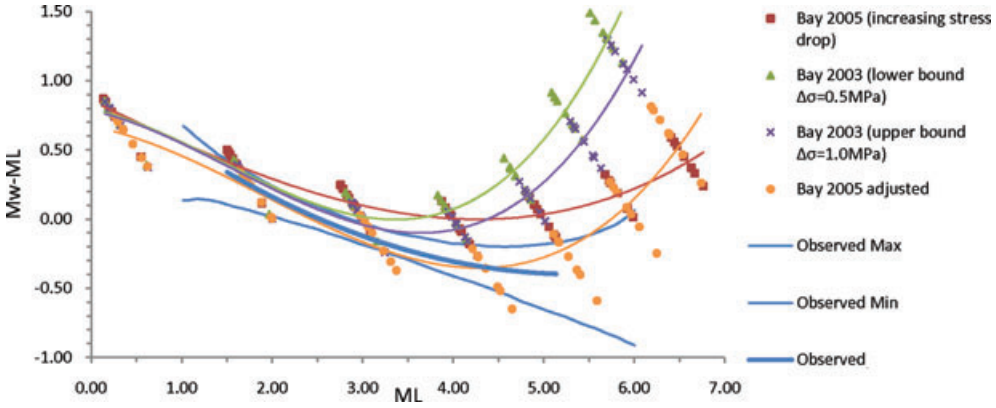

Figure 8. Synthetic M_L–M_W scaling relations based on the Bay *et al*. (2003, 2005) studies along with the adjusted Bay *et al*. (2005) gridsearch results. M_L are computed for a range of distances, resulting in the observed scatter. Third degree polynomials are fit to the data to highlight the trend. The observed M_L–M_W scaling relation is included for comparison.

sensitivity of the M_L–M_W scaling relation to the source and attenuation parameters is therefore explored instead.

5.2 Sensitivity of M_L–M_W scaling to $\Delta\sigma$ and Q

To reconstruct the curvilinear form of the observed M_L–M_W scaling relationship (eq. 17), a non-constant change of ΔA_0 (the change in the amplitude of the synthesized Wood–Anderson Seismogram) with respect to M_W is required. A simple sensitivity test showed that the shape of the scaling relationship was relatively insensitive to the duration of shaking, T_d: doubling the duration of shaking resulted in a decrease of M_L by around 0.1 for all M_W. As T_d has been defined empirically (Bay *et al*. 2003) this was therefore fixed in the simulations. Geometrical spreading, by definition, is independent of M_W and frequency in the case of a point-source simulation. Spherical geometrical spreading in the first 150 km, followed by cylindrical spreading is assumed, consistent with the method for obtaining M_W(SP) applied earlier. Site effects (excluding non-linear effects) are independent of magnitude, but are frequency dependent therefore may affect the shape of the M_L–M_W scaling relationship. The generic rock site amplification function of Boore & Joyner (1997) was tested in the simulations. The site amplification term resulted in a small change in shape of the M_L–M_W scaling relationship, with an increase of 0.3 in M_L for $M_W \approx 1$, dropping linearly down to an increase of 0.2 in M_L for $M_W \approx 6$. Site effects or reference site conditions (Steidl *et al*. 1996) are however, usually available (e.g. Fäh *et al*. 2003b), hence the parameter is fixed in the simulations, as described in the text.

The effect of the site attenuation term κ is analogous to that of stress-drop $\Delta\sigma$ (or source corner-frequency f_c), in that it acts as a low-pass filter, independent of the propagation distance. Due to their similar effects, it is non-trivial to separate $\Delta\sigma$ and κ (e.g. Boore *et al*. 1992), particularly for small magnitude events. We therefore assume a value of κ for the simulations based on other studies. However, it should be noted that increasing the stress-drop is analogous to decreasing the κ value. Furthermore, high κ values can give the impression of an increasing stress-drop with magnitude for small events.

5.3 Effect of $\Delta\sigma$ on M_L–M_W scaling

The effect of the stress-drop on the M_W–M_L scaling relation is shown in Fig. 9. Intrinsic attenuation is not applied in the simulation (specifically $Q = 10^8$ and $\kappa = 0.0$) to analyse only the effect of $\Delta\sigma$. As described by Hanks & Boore (1984), it can be seen that the interaction of the stress-drop and the Wood–Anderson filter plays a strong role in the deviation of the scaling from a linear form. In fact, the stress-drop defines at which point the M_L scale begins to saturate. For $\Delta\sigma$ of 1 MPa, the upper bound of the Bay *et al*. (2003) model, the saturation begins to take effect (i.e. the turning point of the M_W–M_L versus M_L scaling plot in Fig. 9) as early as $M_L = 4$. On the other hand, a $\Delta\sigma$ of 10 MPa delays the start of saturation of M_L to around $M_L = 5$. Extrapolating to larger magnitudes, the 5 MPa stress-drop model is roughly consistent with the maximum M_L value of ~7 suggested by Hanks & Kanamori (1979).

5.4 Effect of Q on M_L–M_W scaling

Published values of Q vary significantly from region-to-region (e.g. Bay *et al*. 2003; Drouet *et al*. 2005, 2008; Edwards *et al*. 2008; Atkinson & Boore 1995; Malagnini *et al*. 2000). One reason for this is the strong covariance of the parameters in eq. (4). To analyse the effect of Q on M_L it is first assumed for simplicity that the high-frequency ω^2 decay of earthquake source spectra (Brune 1970) is not present within the frequency band of recording. The effect of Q alone on the synthesized M_L values can therefore be analysed. To do this, a sufficiently high stress-drop is chosen for the simulations ($\Delta\sigma = 1000$ MPa). The resulting M_L and M_W are shown in Fig. 10(a). For increasing attenuation (decreasing Q), the synthesized M_L values decrease. The effect of changing Q is the same over all magnitudes. This is expected, as Q and, in this case, the source spectral shape (flat in displacement due to the high stress-drop), are both independent of magnitude. In other words, the shape of the displacement spectra at a particular distance from the source is identical for all M_W: only the amplitude differs. In the absence of source spectral decay, intrinsic attenuation is therefore indistinguishable from geometrical decay in terms of its effect on M_L. Finally, it is interesting to note that in the absence of source spectral decay within the recording bandwidth, M_L scales exactly proportional to $1.5M_W$, or alternatively to $\log(M_0)$ rather than 1:1 with M_W (Fig. 10a).

The introduction of a realistic stress-drop (e.g. $\Delta\sigma = 5$ MPa; Allmann & Shearer 2009) appears to diminish the effect of Q at high magnitudes (Fig. 10b). The use of the realistic stress-drop, and hence a source spectrum with high-frequency ω^2 decay within the frequency band of recording, introduces a magnitude

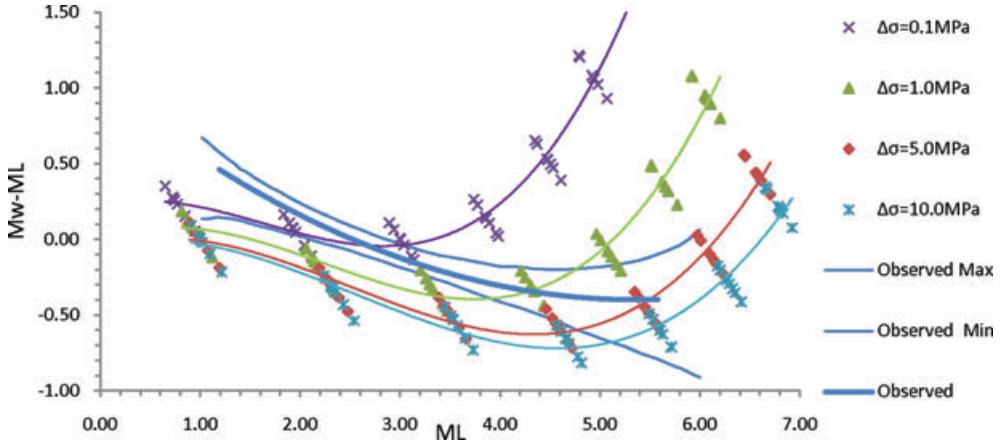

Figure 9. Synthetic M_L–M_W scaling relations for different $\Delta\sigma$ values without attenuation. M_L are computed for a range of distances, resulting in the observed scatter for each M_L. Third degree polynomials are fit to the data to highlight the trend. The observed M_L–M_W scaling relation is included for comparison.

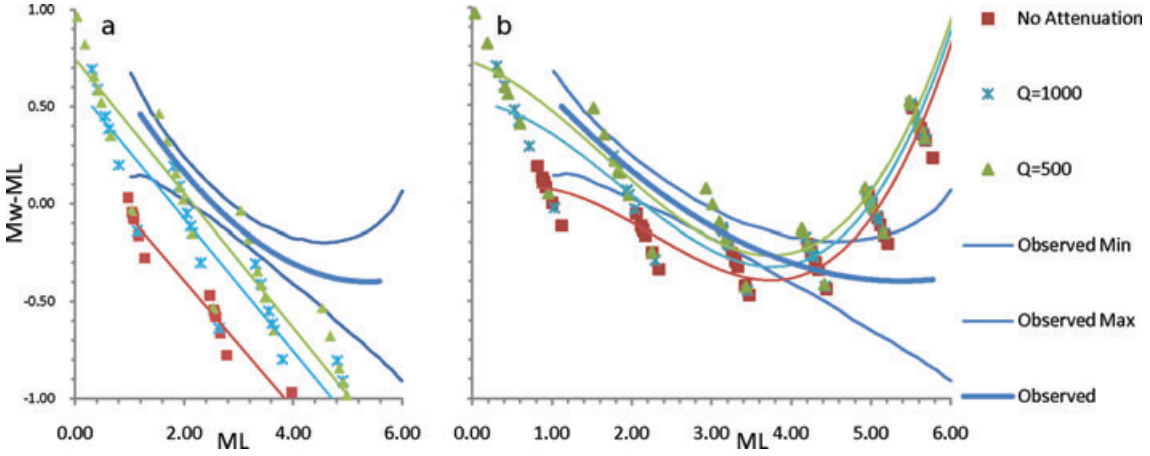

Figure 10. Synthetic M_L–M_W scaling relations for different Q values (a) without influence from the stress-drop (b) with a stress-drop of 5 MPa. M_L are computed for a range of distances, resulting in the observed scatter. Third degree polynomials are fit to the data to highlight the trend—note that in (a) the best fit is linear. The observed M_L–M_W scaling relation is included for comparison.

dependency into the effect of Q on the peak Wood–Anderson amplitude. At low magnitudes, the effect of Q is dominant: the ω^2 decay of the source spectrum begins at a sufficiently high frequency that it does not affect the synthesized peak Wood–Anderson amplitude (as Fig. 10a). However, for increasingly larger magnitudes, the effect of Q becomes less significant as the ω^2 source decay begins at lower frequencies: for a given stress-drop, the corner-frequency of the ω^2 source decay is inversely proportional to the cube of the seismic moment, Brune (1970). As a result of this magnitude dependency, the Q value can change the slope of the M_W–M_L relationship.

5.5 Impact of the M_L–M_W relationship on source scaling

The observed scaling of M_L–M_W can be shown to be due to a combination of the earthquake source spectra (defined by $\Delta\sigma$), the attenuation (defined by the Q value and κ) and the effect of the Wood–Anderson high pass filter. The Q value controls the shape of the scaling relation between M_L and M_W at low magnitudes, while the stress-drop controls the saturation of the M_L scale at high magnitudes. The comparison of the synthetically produced M_L–M_W relation with the observed relation produced for Switzerland can provide an insight into the regional average stress-drop and crustal attenuation. For instance, the observed scaling in this case clearly does not allow for a stress-drop as low as 0.5–1 MPa, as found by Bay *et al*. (2003), throughout the magnitude range (Fig. 8). Furthermore, it suggests that the modification made in Bay *et al*. (2005) is insufficient and the increase of stress-drop with magnitude needs to be stronger still. The variability of stress-drop with magnitude would be consistent with the postulation of Ben-Zion & Zhu (2002) that increasing fault dimensions smooth out the heterogeneity of the tectonic stress-field. The comparison of the observed and synthesised M_L–M_W scaling relation does give us some insight into source and path effects. However, the resolution of source scaling properties is notoriously poor and a detailed analysis in the context of the M_L–M_W scaling relation goes beyond the scope of this paper.

6 SUMMARY AND CONCLUSIONS

It has been shown that the M_W computed using the spectral fitting method presented in this paper are consistent with M_W computed using a moment tensor solution based on broadband waveform fitting of local Swiss earthquakes of $M_W = 2.8$–5.0. The standard deviation of the difference between the two solutions was only 0.06. This error is consistent with the expected error from different moment tensor solutions, for example due to the use of different velocity models, locations, source depths or stations used. Hence we are confident of the magnitude similarity between the spectral and broadband waveform fitting methods. The method was integrated with the automatic picking and location procedure at the SED, and hence provides real-time moment magnitude determination with a delay of about five minutes after automatic waveform pick and earthquake location information are available. Although this is not critical for small events, fast magnitude determination is still important in cases of moderate earthquakes (e.g. $M = 4.5$–6) such that the extent of strong ground shaking can be rapidly assessed. Results are stored in an XML database and are then available on the web in real-time by using an XSL stylesheet. Manual updates to the earthquake location and phase picks are also automatically reprocessed and included when available.

Using the newly computed M_W(SP) a scaling relation between M_L(SED) and M_W was determined. A second degree polynomial was fit to the data and a bootstrap-L1 regression used to robustly determine the scaling law. This law was then applied to M_L for which M_W(MT) were available from independent broadband moment tensor solutions. The old linear scaling law, defined at larger magnitudes ($M_L > 3.5$), was shown to underpredict the smaller broadband moment tensor M_W(MT). The new relation was shown to reduce the magnitude dependence of the residual between predicted and moment tensor M_W(MT). The difference between the two scaling relations is most significant for small magnitude events. For instance, for $M_L = 2.0$, the linear scaling relation predicts $M_W = 1.8$, whereas the quadratic scaling relation defined in this study predicts $M_W = 2.16$. This difference increases for decreasing magnitude. The form of the new relation is similar to a regression of European earthquakes with M_L and M_W by Grünthal & Wahlström (2004) and Grünthal *et al*. (2009), although for $M_L < 3.5$ the relation presented in this study predicts slightly higher M_W.

Theoretically the method detailed in this article should allow determination of M_W on low-cost strong motion networks, as entire spectra are modelled (so high-frequency information can be utilized), and the respective site transfer function (which can be strong

for strong-motion installations) could be removed before processing. This would be useful where broadband data does not exist. However, further tests will be undertaken to assess the robustness of the method in such situations.

The use of a quadratic term in scaling M_L–M_W can cause problems when the magnitude of interest is outside the range of data used in the derivation of the scaling relation. Further work is to be undertaken to incorporate even smaller magnitudes in addition to larger magnitudes into the regression: hence avoiding potential artefacts if the quadratic scaling does not continue to lower or higher magnitudes. This revision of the scaling relation will then be used to obtain a homogeneous moment magnitude scale for the for the forthcoming earthquake catalogue of Switzerland (ECOS09).

Synthesized M_L values were computed for a range of M_W using a stochastic modelling technique. It was shown how the stress-drop and the Q value interact to affect the M_L–M_W scaling relation. The shape of the observed scaling relation could be very closely reconstructed by varying these parameters. The Q value mainly affected low magnitude scaling, while the stress-drop affected high magnitude scaling, specifically the saturation of the M_L scale due to the high-pass Wood–Anderson filter. It was noted that the trade-off between κ and stress-drop meant that the interpretation of increasing stress-drop with magnitude could be substituted with the use of a high κ value. However, κ can be determined from large events which do not exhibit such trade-off (e.g. Anderson & Hough 1984), so κ was fixed based on similar studies for Switzerland. In the absence of ω^2 source spectral decay within the frequency band of interest (i.e. for very small events), M_L scales proportionately to $\log(M_0)$ or $1.5M_W$. At some point, defined by the average stress-drop and therefore the lower frequency limit of the ω^2 spectral decay, this scaling reduces to 1:1 with M_W, followed by the saturation of the M_W scale at higher magnitudes.

ACKNOWLEDGMENTS

Some figures in this paper were produced using GMT 4 (generic mapping tools) software written by Wessel & Smith (1991, 1998). Parts of the code used in creating the inversion tools were provided by Pozo (2004) and Press *et al*. (1997). Thanks to Nicholas Deichmann, Falko Bethmann, Yehuda Ben-Zion, Rachel Abercrombie and the anonymous reviewers for their helpful comments. This work was partly funded by *swissnuclear* within the Pegasos Refinement Project (Renault *et al*. 2010).

Moment magnitudes of Swiss earthquakes were taken from the online database at: http://www.seismo.ethz.ch/mt/RTMT/RTMT_SWISS.php. Only 'class A' events were used. All data used in this study are available via AutoDRM (see http://www.seismo.ethz.ch/autodrm/). Station maps can be obtained from http://www.seismo.ethz.ch/div/links/plots/plots.html.

REFERENCES

Abercrombie, R.E., 1997. Near surface attenuation and site effects from comparison of surface and deep borehole recordings, *Bull. seism. Soc. Am.,* **87,** 731–744.

Abercrombie, R.E. & Leary, P.C., 1993. Source parameters of small earthquakes recorded at 2.5 km depth, Cajon Pass, southern California: implications for earthquake scaling, *Geophys. Res. Lett.,* **20,** 1511–1514.

Aki, K. & Richards, P., 1980. *Quantitative Seismology,* W.H. Freeman, New York.

Allmann, B.P. & Shearer, P.M., 2007. Spatial and temporal stress drop variations in small earthquakes near Parkfield, California, *J. geophys. Res.,* **112,** B04305, doi:10.1029/2006JB004395.

Allmann, B.P. & Shearer, P.M., 2009. Global variations of stress drop for moderate to large earthquakes, *J. geophy. Res.,* **114,** B01310, doi:10.1029/2008JB005821.

Anderson, J.G. & Hough, S.E., 1984. A model for the shape of the Fourier amplitude spectrum of acceleration at high frequencies, *Bull. seism. Soc. Am.,* **74,** 1969–1993.

Atkinson, G.M. & Boore, D.M., 1995. Ground-motion relations for eastern North America, *Bull. seism. Soc. Am.,* **85,** 17–30.

Baer, M. *et al*., 2007. Earthquakes in Switzerland and surrounding regions during 2006, *Eclogae Geologicae Helvetiae,* **100**(3), 517–528.

Bay, F., Fäh, D., Malagnini, L. & Giardini, D., 2003. Spectral shear-wave ground-motion scaling in Switzerland, *Bull. seism. Soc. Am.,* **93,** 414–429.

Bay, F., Wiemer, S., Fäh, D. & Giardini, D., 2005. Predictive ground motion scaling in Switzerland: best estimates and uncertainties, *J. Seismol.,* **9,** 223–240.

Ben-Zion, Y. & Zhu, L., 2002. Potency-magnitude scaling relations for Southern California earthquakes with $1.0 < ML < 7.0$, *Geophys. J. Int.,* **148,** F1–F5.

Bernardi, F., Braunmiller, J., Kradolfer, U. & Giardini, D., 2004. Automatic regional moment tensor inversion in the European-Mediterranean region, *Geophys. J. Int.,* **157,** 703–716.

Bommer, J.J., Stafford, P.J., Alarcon, J.E. & Akkar, S., 2007. The influence of magnitude range on empirical ground-motion prediction, *Bull. seism. Soc. Am.,* **97,** 2152–2170.

Boore, D., 2003. Simulation of ground motion using the stochastic method, *Pure appl. Geophys.,* **160**(3–4), 635–676.

Boore, D.M. & Boatwright, J., 1984. Average body-wave radiation coefficients, *Bull. seism. Soc. Am.,* **74,** 1615–1621.

Boore, D.M. & Joyner, W.B., 1997. Site amplifications for generic rock sites, *Bull. seism. Soc. Am.,* **87,** 327–341.

Boore, D., Joyner, W.B. & Wennerberg, L., 1992. Fitting the stochastic ω^{-2} source model to observed response spectra in western North America: trade-offs between $\Delta\sigma$ and κ, *Bull. seism. Soc. Am.,* **82,** 1956–1963.

Braunmiller, J., Deichmann, N., Giardini, D. & Wiemer, S.; and the SED Magnitude Working Group, 2005. Homogeneous moment-magnitude calibration in Switzerland, *Bull. seism. Soc. Am.,* **95,** 58–74.

Brune, J.N., 1970. Tectonic stress and the spectra of seismic shear waves from earthquakes, *J. geophys. Res.,* **75,** 4997–5010.

Brune, J.N., 1971. Correction: tectonic stress and the spectra of seismic shear waves from earthquakes, *J. geophys. Res.,* **76,** 5002.

Clinton, J.F., Hauksson, E. & Solanki, K., 2006. An evaluation of the SCSN moment tensor solutions: robustness of the M-w magnitude scale, style of faulting, and automation of the method, *Bull. seism. Soc. Am.,* **96,** 1689–1705.

Cotton, F., Pousse, G., Bonilla, F. & Scherbaum, F., 2008. On the discrepancy of recent European ground-motion observations and predictions from empirical models: analysis of KiK-net accelerometric data and point-sources stochastic simulations, *Bull. seism. Soc. Am.,* **98,** 2244–2261.

Deichmann, N., 2006. Local magnitude, a moment revisited, *Bull. seism. Soc. Am.,* **96,** 1267–1277.

Dreger, D.S., 2003. TDMT_INV: time domain seismic moment tensor INVersion, *Int. Handbook Earthq. Eng. Seismol.,* **81B,** 1627.

Drouet, S., Chevrot, S., Cotton, F. & Souriau, A., 2008. Simultaneous inversion of source spectra, attenuation parameters, and site responses: application to the data of the French accelerometric network, *Bull. seism. Soc. Am.,* **98,** 198–219.

Drouet, S., Cotton, F. & Souriau, A., 2005. Attenuation, seismic moments, and site effects for weak motion events. Application to the Pyrenees, *Bull. seism. Soc. Am.,* **95,** 1731–1748.

Edwards, B., 2008. On the use of micro-earthquakes to predict strong ground-motion, *PhD thesis*, University of Liverpool.

Edwards, B. & Rietbrock, A., 2009. A comparative study on attenuation and source-scaling relations in the Kanto, Tokai, and Chubu regions of Japan, using data from Hi-Net and Kik-Net, *Bull. seism. Soc. Am.,* **99,** 2435–2460, doi:10.1785/0120080292.

Edwards, B., Rietbrock, A., Bommer, J.J. & Baptie, B., 2008. The acquisition of source, path and site effects from micro-earthquake recordings using Q tomography: application to the UK, *Bull. seism. Soc. Am.,* **98,** 1915–1935.

Eshelby, J.D., 1957. The determination of an elastic field of an ellipsoidal inclusion and related problems, *Proc. R. Soc. Lond. A,* **241,** 376–396.

Fäh, D. *et al*., 2003a. Earthquake Catalogue Of Switzerland (ECOS) and the related macroseismic database, *Eclogae Geologicae Helvetiae,* **96,** 219–236.

Fäh, D., Kind, F. & Giardini, D., 2003b. Inversion of local S-wave velocity structures from average H/V ratios, and their use for the estimation of site-effects. *J. seismol.,* **7,** 449–467.

Grünthal, G. & Wahlström, R., 2004. An M_W based earthquake catalogue for central, northern and northwestern Europe using a hierarchy of magnitude conversions, *J. Seismol.,* **7,** 507–531.

Grünthal, G., Wahlström, R. & Stromeyer, D., 2009. The unified catalogue of earthquakes in central, northern, and northwestern Europe (CENEC)-updated and expanded to the last millennium Source, *J. Seismol.,* **13,** 517–541.

Gutenberg, B. & Richter, C.F., 1954. *Seismicity of the Earth and Associated Phenomena,* 2nd edn, Princeton University Press, Princeton, New Jersey. Kanamori and Jennings, 1978.

Hanks, T.C., 1982. Fmax, *Bull. seism. Soc. Am.,* **72,** 1867–1880.

Hanks T.C. & Boore, D., 1984. Moment-magnitude relations in theory and practice, *J. geophys. Res.,* **89,** 6229–6235.

Hanks, T.C. & Kanamori, H., 1979. A moment magnitude scale. *J. geophys. Res.,* **84**(B5), 2348–2350.

Ide, S., Beroza, G.C., Prejean, S.G. & Ellsworth, W.L., 2003. Apparent break in earthquake scaling due to path and site effects on deep borehole recordings, *J. geophy. Res.,* **108,** B5, 2271.

Kisslinger C., 1980. Evaluation of S to P amplitude ratios for determining focal mechanisms from regional network observations, *Bull. seism. Soc. Am.*, **70,** 999–1014.

Kisslinger C., Bowman, R. & Koch, K., 1981. Procedures for computing focal mechanisms from local (SV/P) data, *Bull. seism. Soc. Am.,* **71,** 1719–1729.

Kradolfer, U., 1984. Magnitudenkalibrierung von Erdbebenstationen in der Schweiz, *Diploma thesis*. ETH Zurich.

Lees, J.M. & Park, J., 1995. Multiple-taper spectral analysis: a stand-alone C subroutine, *Comput. Geosci.,* **21,** 199–236.

Madariaga, R., 1976. The dynamics of an expanding circular fault, *Bull. seism. Soc. Am.,* **66,** 639–666.

Malagnini, L., Herrmann, R.B. & Koch, K., 2000. Regional ground-motion scaling in central Europe, *Bull. seism. Soc. Am.,* **90,** 1052–1061.

Mayeda, K. & Malagnini, L., 2010. Source radiation invariant property of local and near-regional shear-wave coda: application to source scaling for the M-w 5.9 Wells, Nevada sequence, *Geophys. Res. Lett.,* **37,** L07306, doi:10.1029/2009GL042148.

Mayeda, K. & Walter, W.R., 1996. Moment, energy, stress drop, and source spectra of western United States earthquakes from regional coda envelopes, *J. geophys. Res.,* **101,** 11195–11208.

Miller, S.A., Ben-Zion, Y. & Burg, J.-P., 1999. A three-dimensional fluid controlled earthquake model: behaviour and implications, *J. geophys. Res.,* **104,** 10621–10638.

BSSC, Building Seismic Safety Council, 2003. The 2003 NEHRP Recommended provisions for new buildings and other structures, Part 1: provisions (FEMA 450), www.bssconline.org.

Newmark, N.M., & Hall, W.J., 1982. *Earthquake Spectra and Design,* Monograph prepared for Earthquake Engineering Research Institute, Berkeley, California.

Ottemöller, L., 2002. Lg wave Q tomography in Central America, *Geophys. J. Int.,* **150,** 295–302.

Ottemöller, L. & Havskov, J., 2003. Moment magnitude determination for local and regional earthquakes based on source spectra, *Bull. seism. Soc. Am.,* **93,** 203–214.

Park, J., Lindberg, C.R. & Vernon, F.L., 1987. Multitaper spectral analysis of high frequency seismograms, *J. geophys. Res.,* **92,** 12675–12684.

Poggi, V., Edwards, B. & Fäh, D., 2010. Derivation of a reference shear-wave velocity model from empirical site amplification, *Bull. seism. Soc. Am.*, in press, doi:10.1785/0120100060.

Pozo, R., 2004. Template numerical toolkit, [online]. Available at: http://math.nist.gov/tnt/ (May 2009).

Press, W.H., Teukolsky, S.A., Vetterling, W.T. & Flannery, B.P., 1997. *Numerical Recipes in C: The Art of Scientific Computing,* 2nd edn, Cambridge University Press, pp. 278–281, 288–290, 417–424, and 515–518.

Raoof, M., Herrmann, R.B. & Malagnini, L., 1999. Attenuation and excitation of three component ground motion in southern California, *Bull. seism. Soc. Am.,* **89,** 888–902.

Renault, P., Heuberger, S. & Abrahamson, N.A., 2010. PEGASOS Refinement Project: an improved PSHA for Swiss nuclear power plants, in *Proceedings of 14ECEE – European Conference of Earthquake Engineering*, Ohrid, Republic of Macedonia, Paper ID 991.

Rietbrock, A. 2001. P wave attenuation structure in the fault area of the 1995 Kobe earthquake, *J. geophys. Res.,* **106,** 4141–4154.

Sonley, E. & Abercrombie, R.E., 2006. Effects of methods of attenuation correction on source parameter determination, in *Earthquakes: Radiated Energy and the Physics of Faulting*. Geophys. Monogr. Ser., Vol. 170, pp. 91–97, eds Abercrombie, R.E., McGarr, A., Kanamori, H. & Di Toro, G., American Geophysical Union, Washington, D.C.

Steidl, J.H., Tumarkin, A.G. & Archuleta, R.J., 1996. What is a reference site?, *Bull. seism. Soc. Am.,* **86,** 1733–1748.

Uhrhammer, R.A. & Collins, E.R., 1990. Synthesis of Wood Anderson seismograms from broadband digital records, *Bull. seism. Soc. Am.,* **80,** 702–716.

Viegas, G., Abercrombie, R.E. & Kim, W.-Y., 2010. The 2002 M5 Au Sable Forks, NY, earthquake sequence: source scaling relationships and energy budget. *J. geophys. Res.,* **115**, B07310, doi:10.1029/2009JB006799.

Wessel, P. & Smith, W.H.F., 1991. Free software helps map and display data. *EOS Trans. Am. geophys. Un.,* **72,** 441, 445–446.

Wessel, P. & Smith, W.H.F., 1998. New, improved version of the Generic Mapping Tools Released, *EOS Trans. Am. geophys. Un.,* **79,** 579.

Woessner, J. & Wiemer, S., 2005. Assessing the quality of earthquake catalogues: estimating the magnitude of completeness and its uncertainty, *Bull. seism. Soc. Am.,* **95,** 684–698.